Sensing matrix prediction from back-scattered data in computational microwave imaging

Published in:
IEEE Antennas and Wireless Propagation Letters

Document Version:
Peer reviewed version

Queen's University Belfast - Research Portal:
Link to publication record in Queen's University Belfast Research Portal

Sensing Matrix Prediction from Back-scattered Data in Computational Microwave Imaging

Jiaming Zhang, *Graduate Student Member, IEEE,* Rahul Sharma, *Member, IEEE,* Guillermo
Álvarez-Narciandi, *Member, IEEE,* María García-Fernández, *Member, IEEE,* Muhammad Ali Babar
Abbasi, *Member, IEEE,* and Okan Yurduseven, *Senior Member, IEEE*

Abstract—In this paper, the challenge of enhancing the efficiency of computational imaging (CI) at microwave frequencies is addressed. While CI simplifies the hardware complexity of conventional microwave imaging techniques, it requires the knowledge of a sensing matrix that is governed by the aperture radiated fields. This can be a computationally expensive process. As a drastic alternative to this conventional approach, a Pix2pix conditional generative adversarial network (cGAN) is introduced to learn the intricate relationship between the back-scattered measurements from the imaging scene and the sensing matrix of the imaging system. The proposed network yields high-fidelity estimations with minimized error and achieves a remarkable reduction in the time required to compute the sensing matrix. This advancement holds significant potential for improving the overall efficiency of microwave CI techniques, addressing both hardware complexity and computational burdens.

Index Terms—Computational imaging, deep learning, sensing matrix, microwave imaging.

I. INTRODUCTION

IMAGING at microwave frequencies has attracted significant attention due to its ability to penetrate optically opaque materials using non-ionizing electromagnetic (EM) waves. Synthetic aperture radar (SAR) is one of the most important techniques used in conventional microwave imaging [1], [2]. Although SAR-based systems can provide good-quality image reconstructions, such methods still have several challenges, including a slow data acquisition process and increased hardware complexity due to the raster scan requirement [3]. An alternative technique which can improve the data acquisition speed is computational imaging (CI), enabled by the use of coded-apertures [4]–[6]. A major benefit of CI-based systems is that the volume of data acquisition channels can be reduced significantly, decreasing the hardware complexity [7]. This is because the coded-aperture-based antennas used in CI systems are capable of encoding the scene information onto a series of quasi-random and spatially-incoherent radiation patterns (or measurement modes) [8], achieving a physical layer compression. The acquired back-scattered measurements from the scene can be systematically associated with the underlying scene information through the transfer function of

the CI system, referred to as the sensing (or measurement) matrix [9]. Leveraging the CI concept, although the hardware complexity can be reduced, this simplification comes at the cost of an increased burden in the signal processing layer. This is because, due to the indirect nature of scene information collection in CI, the image reconstruction from the compressed measurements demands the processing of large sensing matrices, drastically increasing the computational burden [10], [11].

An alternative solution for computing the sensing matrix can be considered in the context of employing deep learning techniques. Previous studies related to sensing matrix estimations through deep learning methodologies used reconstructed images as inputs, which is potentially a challenging task [12]–[14]. This is due to the significant amount of time needed to accomplish the prior reconstructions of the scene as a prerequisite for sensing matrix prediction. [15] proposed a solution to circumvent the need to use the reconstructed images to predict the sensing matrix. Instead, it demonstrated that the coded-aperture field distribution can directly be used to predict the corresponding sensing matrices. Whereas this is a promising idea, having the aperture field distribution available is not always possible and measuring it requires a significant time and effort. This is because it requires a highly-sensitive and time-consuming near-field scan process [16]. To address these challenges, an alternative technique is needed. In this work, we propose a new technique to estimate the sensing matrix directly from back-scattered measurements acquired with a CI system. Our method exclusively regards the back-scattered measurement as the input of the proposed network, eliminating the need for scene reconstruction and for measuring the radiation patterns by near-field scanning. To the best of our knowledge, this is the first time that a deep learning technique is developed to estimate the sensing matrix directly from the back-scattered microwave CI measurements. Results show that the sensing matrices can be accurately learned, enabling the restoration of similar magnitudes and phases (comparable with those sensing matrices computed using conventional, computationally expensive methods).

II. CONVENTIONAL METHOD AND PROPOSED NETWORK

A. Compressive Computational Microwave Imaging

Following the first Born approximation [17]–[19], the scattered field, E_{scat}, contains the reflectivity information of each pixel of the scene, $\rho(\mathbf{r})$ [20]:

$$E_{scat} = \int_S \rho(\mathbf{r})E_{inc}(\mathbf{r})dS, \tag{1}$$

where r indicates the coordinates vector of each pixel of the scene, S denotes the surface, and E_{inc} is the incident field from the aperture. We note that, in this work, the bold font is used to denote the vector-matrix notation.

The transmitter and receiver apertures can be modelled leveraging a set of equivalent sources, each representing a radiating element across the aperture [9]. In particular, each aperture is discretized into N_s equivalent sources, and the radiated field corresponding to the m-th measurement mode at a point r of the scene is given by:

$$\mathbf{E}(m, \mathbf{r}) = \sum_{s=1}^{N_s} \frac{\boldsymbol{\alpha}_{m,s}}{\|\mathbf{r}'_s - \mathbf{r}\|} e^{-j\frac{2\pi f}{c}\|\mathbf{r}'_s - \mathbf{r}\|}, \quad (2)$$

where f is the imaging frequency, and c is the speed of light in free-space. Furthermore, $\boldsymbol{\alpha}_{m,s}$ denotes the aperture field value of the s-th equivalent source (located at $\mathbf{r}'_s$) for the m-th measurement mode. The sensing matrix, $\mathbf{H}$, is derived by performing a dot product between the fields radiated by the transmitter and the receiver apertures, $\mathbf{E}_{tx}$ and $\mathbf{E}_{rx}$, respectively [21], as follows:

$$\mathbf{H} = \mathbf{E}_{tx} \cdot \mathbf{E}_{rx}. \quad (3)$$

The signal measured at the receiver, which is also called the back-scattered measurement, $\mathbf{g}$, is given by:

$$\mathbf{g} = \mathbf{H}\boldsymbol{\rho}. \quad (4)$$

The back-scattered measurement, $\mathbf{g}$, is a vector of size $M \times 1$, where M is the number of measurement modes, and the sensing matrix has size $M \times N$, where N is the number of pixels in the imaging scene. This suggests that the sensing matrix is not necessarily square, i.e., $N \neq M$. To estimate the reflectivity of the scene, $\boldsymbol{\rho}_{rec}$, it is possible to use different techniques, such as matched filtering [18]:

$$\boldsymbol{\rho}_{rec} = \mathbf{H}^\dagger \mathbf{g}, \quad (5)$$

where $\mathbf{H}^\dagger$ denotes the conjugate transpose of the sensing matrix. For the studied microwave CI scenario, the main parameters of the imaging setup are outlined in Table I whereas the imaging configuration is depicted in Fig. 1.

TABLE I
PARAMETERS OF THE IMAGING SYSTEM AND THE IMAGING SCENE.

Transmitting Aperture Size	10.0 λ × 10.0 λ
Receiving Aperture Size	10.0 λ × 10.0 λ
Number of Equivalent Sources on Each Aperture	400
Gap between Transmitter and Receiver	2.5 λ
Imaging Distance	15.0 λ
Scene Size	5.0 λ × 5.0 λ
Imaging Frequency	18 GHz
Number of Pixels of the Scene	256

B. Data Generation

For the studied CI system depicted in Fig. 1, we consider scenarios with an upper bound limit of the signal-to-noise-ratio (SNR) below 30 dB. As a result, the number of measurement modes is considered to be 64, which is found to be optimal
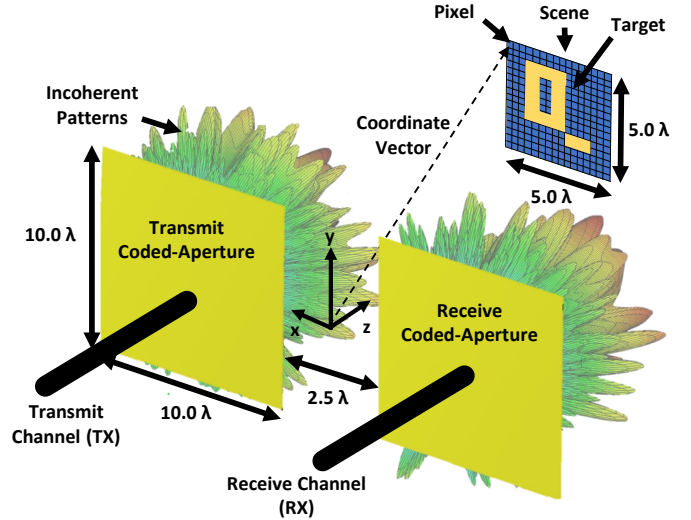

Fig. 1. Coded-aperture CI setup operating in a bi-static mode that is used for dataset generation. The target "Q" is the calibration imaging target.
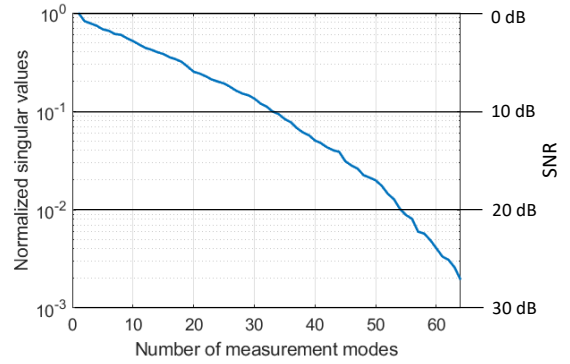

Fig. 2. Singular value spectrum for the imaging system.

utilizing a Singular Value Decomposition (SVD) analysis [22] as shown in Fig. 2. Thus, the total number of measurement modes is $M = 64$, which is significantly smaller than the number of pixels in the scene, $N = 256$. Hence, the scene is undersampled ($M < N$).

According to (2) and (3), different radiating element distributions help with the generation of different sensing matrix samples. Fig. 3 summarizes the process of generating samples of sensing matrices. Referring to (4), the back-scattered measurements contain the information of the related sensing matrix and the scene. Because the reflectivity of the targets has no relationship with the sensing matrix, to avoid redundant information from the reflectivity affecting the optimization of the proposed network, the back-scattered measurements are considered as the only input in the proposed network. However, to generate the data for the sensing matrix prediction, a calibration target is necessary. According to (4), a variation in the back-scattered measurement samples is due to the changing of the sensing matrix when a single calibration

Fig. 3. Different distributions of the radiating elements yield different sensing matrices.
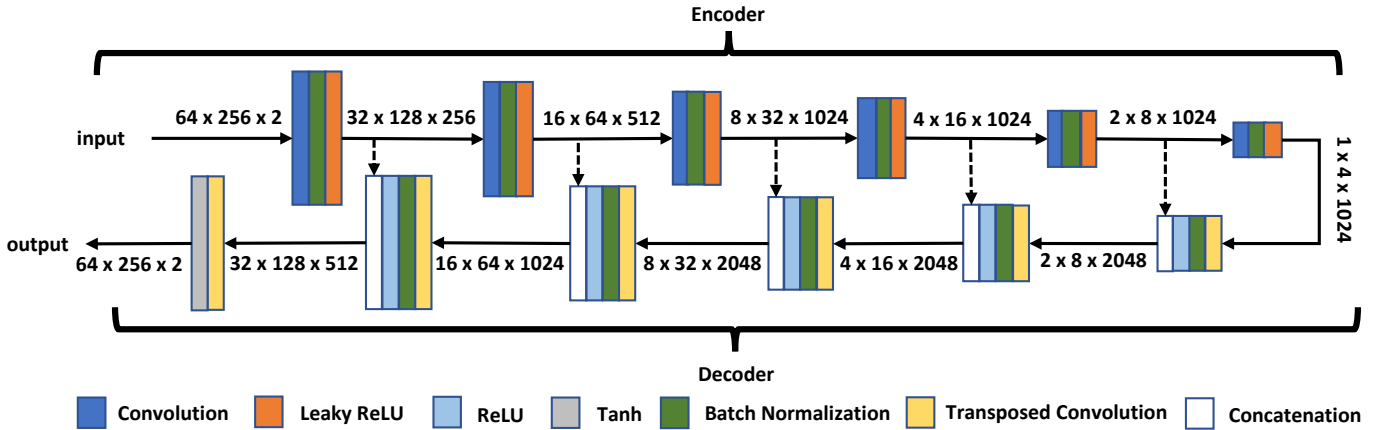
Encoder

Fig. 4. The generator network is composed of a downsampling encoder and an upsampling decoder.

target is utilized. Hence, each training and testing sample pair consists of a sensing matrix and the corresponding back-scattered measurement.

C. Network Architecture and Optimization

The Pix2pix conditional generative adversarial network (cGAN) consists of two convolutional neural networks (CNNs) [23]–[25]: one is defined as the generator, while the other one is defined as the discriminator. The generator generates the output based on the input information, while the discriminator is employed to determine whether the predicted output is similar to the ground truth. In this scenario, the network learns the mapping between the back-scattered measurements and the sensing matrices. Hence, the back-scattered measurements are not only the inputs to the generator but also the input condition for the proposed discriminator in this paper.

As depicted in Fig. 4, the generator consists of an encoder, which downsamples the feature maps, and a decoder, which upsamples the compressed feature maps. The five layers in the decoder are equipped with 256, 512, 1024, 1024 and 1024 CNN filters, while the encoder has one more layer with 1024 CNN filters, as shown in Fig. 4. The concatenated layer that connects the encoder with the decoder is called the "skip connection", which can enhance the gradient propagation [26], [27]. The encoder uses a leaky rectified linear unit (ReLU) [28], [29] as the activation function, while the decoder uses a ReLU as the activation function. The discriminator has the same layer architecture as the encoder of the generator. In addition, to classify the generated image as either real or fake, the output layer consists of a convolutional layer with a single filter of size 1×1 with a Tanh activation function [30]–[32]. For the discriminator, the inputs are the back-scattered measurements and the original or the predicted sensing matrices, while the output is the probability that the input sensing matrix is original.

As both the sensing matrices and the back-scattered measurements are complex-valued, the real and the imaginary parts are separated into two channels in the Pix2pix cGAN [33]. To address the problem of size mismatch between the back-scattered measurements and the input size, the back-scattered measurements are formatted to align with the input size of

the generator through the application of zero-padding [34]. The loss functions for the generator and the discriminator are the same as proposed in [23]. The proposed Pix2pix cGAN uses the Adam optimizer [35] for the training process and the weights are initialized using the Xavier uniform initialization technique [36]. For the training process, a training dataset of 88,000 training sample pairs of back-scattered measurements and sensing matrices is employed to help the proposed Pix2pix cGAN to learn the features of the back-scattered measurements for accurate predictions. For the testing process, the trained Pix2pix cGAN will be evaluated for its predicting performance by making use of a testing dataset.

III. NUMERICAL RESULTS AND DISCUSSION

To validate the accuracy of the sensing matrix prediction, a comparison between the original (ground truth) sensing matrices and the predicted (learned) sensing matrices is shown in Fig. 5. For the study presented in Fig. 5, three groups of different sensing matrices are considered. The NMSE [37] is also calculated to evaluate the fidelity of the predicted sensing matrices. Observing Fig. 5, it can be seen that, qualitatively, the predicted sensing matrices exhibit good agreement with the original sensing matrices calculated using (2) and (3). Table II shows a quantitative assessment of this comparison, where the NMSE is below 0.0228 for all three cases. Moreover, using the proposed prediction technique, the computation time is reduced by up to 1.014 s as compared to the conventional calculation of the sensing matrices. To evaluate the predicting performance of the cGAN, a testing dataset of 1,000 testing sample pairs is leveraged. The above results are also obtained by three sample pairs randomly chosen from the testing dataset. With the testing dataset, the average NMSE of prediction is 0.0230, and the average calculation time is reduced from 1.315 s (using (2) and (3) to calculate a sensing matrix) to 0.352 s (using the proposed generator to predict the sensing matrix when a back-scattered measurement is presented) on a Python platform running on an Intel (R) Core (TM) i7-1265U CPU. In addition to the significant advantage of the proposed technique to eliminate the need for measuring the aperture fields, these results show a reduction of 73.3% in the computation time while preserving the fidelity of the sensing matrices.
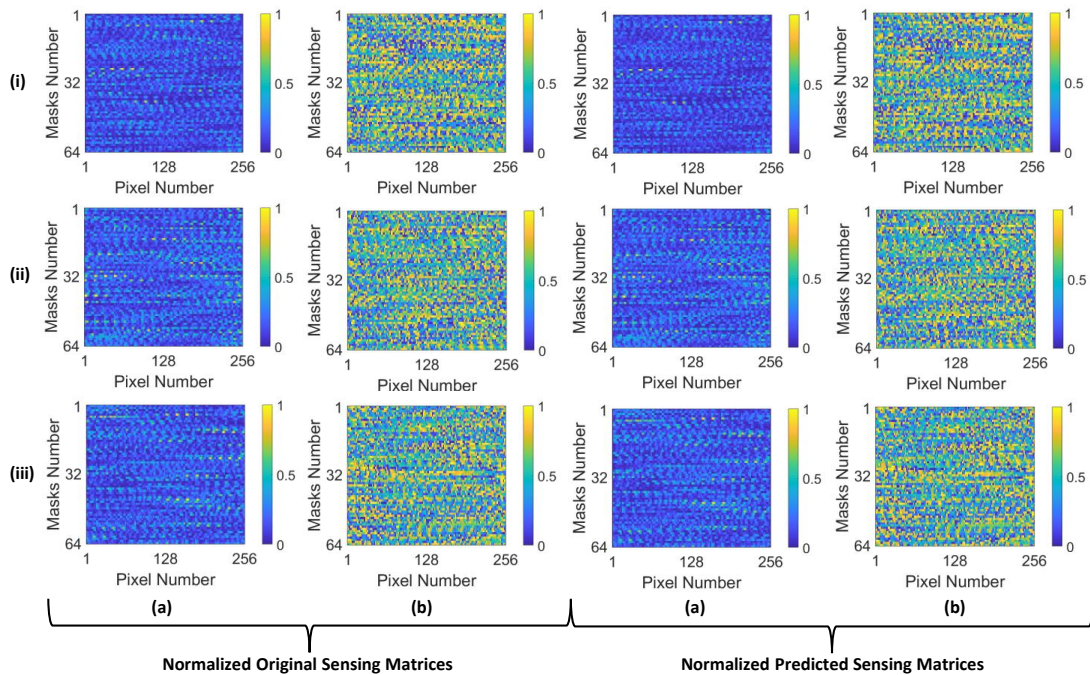
Fig. 5. There are three groups of sensing matrices, identified as (i), (ii) and (iii). Comparison between (a) the normalized magnitudes and (b) the normalized phases of the sensing matrices obtained with conventional method and the predicted sensing matrices retrieved with the proposed generator is shown.
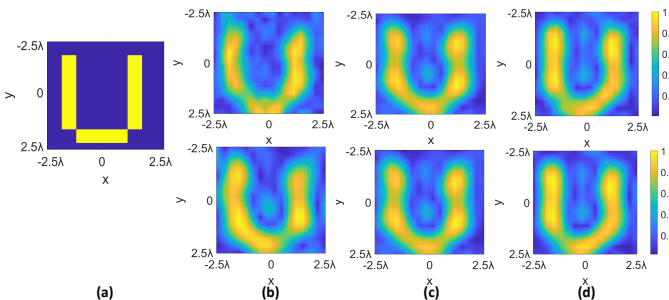

Fig. 6. Comparison of the reconstructed images. Top row: Images reconstructed using the predicted sensing matrix. Bottom row: Images reconstructed using the corresponding original sensing matrix. (a) Imaged target, reconstructed images with (b) 15 dB SNR, (c) 20 dB SNR and (d) without noise.

quality of reconstructed images decreases as the SNR level is reduced. This can be appreciated by analyzing the SVD plot provided in Fig. 2, where the system provides fewer useful measurement modes (i.e. the number of measurement modes that remain above the SNR level) as the SNR level is reduced. Moreover, the specific values of NMSEs for the reconstructed images shown in Fig. 6 are given in Table III. Table III shows that the NMSE values between the image reconstructions and the target remain comparable regardless of using the predicted sensing matrix or the original sensing matrix. Hence, these results suggest that the proposed network can provide similar results as the conventional method under a noisy environment.

TABLE II
NUMERIC RESULTS FOR THREE PREDICTED SENSING MATRICES

Sensing Matrices	(i)	(ii)	(iii)
NSME between Sensing Matrices	0.0228	0.0189	0.0224
Computation Time Reduced	0.979 s	1.014 s	0.983 s

TABLE III
NMSE OF IMAGE RECONSTRUCTIONS BASED ON THE PREDICTED
SENSING MATRIX AND THE ORIGINAL SENSING SHOWN IN FIG. 6.

Noise Level	Conventional Method	Proposed Method
15 dB	0.4952	0.5063
20 dB	0.4323	0.3899
Without Noise	0.3842	0.3779

After estimating the sensing matrices, the reconstructed images can be generated based on (5). For the imaging process, the parameters listed in Table I and the U-shaped target shown in Fig. 6 are utilized. The approach's practicality and robustness are evaluated through a noise analysis, studying the learning model's performance in noisy conditions. To this end, different levels of Gaussian white noise were added to the back-scattered measurements, g [38]. Gaussian white noise is considered in this scenario because it exhibits a close alignment with the statistical attributes observed in various noise typologies encountered within radar systems [39], [40]. Fig. 6 shows the reconstructed images with no noise as well as at 15 dB and 20 dB SNR levels of the back-scattered measurements, respectively. Analyzing Fig. 6, it can be observed that the

IV. CONCLUSION

In this article, a Pix2pix cGAN was developed to improve the computation efficiency of the sensing matrix for coded-aperture-based microwave CI systems. The proposed Pix2pix cGAN accurately predicts the CI system's sensing matrix by learning the features of the back-scattered measurements. On 1,000 testing samples, the average NMSE scores of the predicted matrices were found to be 0.0230. Furthermore, a significant reduction in computation time, calculated to be 73.3% on average, was achieved. This development offers the potential to enhance the overall efficiency of CI at microwave frequencies, which can be particularly useful for three-dimensional imaging [41], tackling challenges related to hardware complexity and computational loads.

REFERENCES

[1] D. M. Sheen, D. L. McMakin, and T. E. Hall, "Three-dimensional Millimeter-wave Imaging for Concealed Weapon Detection," *IEEE Trans. Microw. Theory Tech.*, vol. 49, pp. 1581–1592, 2001.

[2] J. A. Martinez-Lorenzo, F. Quivira, and C. Rappaport, "SAR Imaging of Suicide Bombers Wearing Concealed Explosive Threats," *Prog. Electromagn. Res.*, vol. 125, pp. 255–272, 2012.

[3] R. Sharma, O. Yurduseven, B. Deka, and V. Fusco, "Hardware Enabled Acceleration of Near-Field Coded Aperture Radar Physical Model for Millimetre-Wave Computational Imaging," *Prog. Electromagn. Res. B*, vol. 90, pp. 91–108, 2021.

[4] T. Fromenteze, O. Yurduseven, M. F. Imani, J. Gollub, C. Decroze, D. Carsenat, and D. R. Smith, "Computational Imaging Using A Mode-mixing Cavity At Microwave Frequencies," *Appl. Phys. Lett.*, vol. 106, no. 19, p. 194104, 2015.

[5] D. Brady, *Optical Imaging and Spectroscopy*. Wiley, 2009.

[6] R. Barrett, M. Berry, T. Chan, J. Demmel, J. Donato, J. Dongarra, V. Eijkhout, R. Pozo, C. Romine, and H. Vorst, "Templates for the Solution of Linear Systems: Building Blocks for Iterative Methods, 2nd Edition," in *Templates for the Solution of Linear Systems: Building Blocks for Iterative Methods, 2nd Edition*. SIAM, 1994.

[7] M. F. Imani, J. N. Gollub, O. Yurduseven, A. V. Diebold, M. Boyarsky, T. Fromenteze, L. Pulido-Mancera, T. Sleasman, and D. R. Smith, "Review of Metasurface Antennas for Computational Microwave Imaging," *IEEE Trans. Antennas Propag.*, vol. 68, no. 3, pp. 1860–1875, 2020.

[8] T. Sleasman, M. F. Imani, J. N. Gollub, and D. R. Smith, "Dynamic Metamaterial Aperture for Microwave Imaging," *Appl. Phys. Lett.*, vol. 107, no. 20, p. 204104, 2015.

[9] G. Lipworth, A. Rose, O. Yurduseven, V. R. Gowda, M. F. Imani, H. Odabasi, P. Trofatter, J. Gollub, and D. R. Smith, "Comprehensive simulation platform for a metamaterial imaging system," *Appl. Opt.*, vol. 54, no. 31, pp. 9343–9353, 2015.

[10] O. Yurduseven, J. N. Gollub, A. Rose, D. L. Marks, and D. R. Smith, "Design and Simulation of a Frequency-Diverse Aperture for Imaging of Human-Scale Targets," *IEEE Access*, vol. 4, pp. 5436–5451, 2016.

[11] J. N. Gollub, O. Yurduseven *et al.*, "Large Metasurface Aperture for Millimeter Wave Computational Imaging at the Human-Scale," *Sci Rep*, vol. 7, 2017.

[12] W. Cui, F. Jiang, X. Gao, W. Tao, and D. Zhao, "Deep Neural Network Based Sparse Measurement Matrix for Image Compressed Sensing," in *Proc. IEEE Int. Conf. on Image Process. (ICIP)*, 2018, pp. 3883–3887.

[13] R. Mdrafi and A. C. Gurbuz, "Joint Learning of Measurement Matrix and Signal Reconstruction via Deep Learning," *IEEE Trans. Comput. Imaging*, vol. 6, pp. 818–829, 2020.

[14] S. Li, W. Zhang, Y. Cui, H. V. Cheng, and W. Yu, "Joint Design of Measurement Matrix and Sparse Support Recovery Method via Deep Auto-Encoder," *IEEE Signal Process. Lett.*, vol. 26, no. 12, pp. 1778–1782, 2019.

[15] J. Zhang, R. Sharma, M. García-Fernández, G. Álvarez Narciandi, M. A. B. Abbasi, and O. Yurduseven, "Deep Learning for Sensing Matrix Prediction in Computational Microwave Imaging With Coded-Apertures," *IEEE Access*, vol. 12, pp. 16 844–16 855, 2024.

[16] T. Sleasman, M. F. Imani, O. Yurduseven, K. P. Trofatter, V. R. Gowda, D. L. Marks, J. N. Gollub, and D. R. Smith, "Near Field Scan Alignment Procedure for Electrically Large Apertures," *IEEE Trans. Antennas Propag.*, vol. 65, no. 6, pp. 3257–3262, 2017.

[17] J. Hunt, T. Driscoll, A. Mrozack, G. Lipworth, M. Reynolds, D. Brady, and D. R. Smith, "Metamaterial Apertures for Computational Imaging," *Science*, vol. 339, no. 6117, pp. 310–313, 2013.

[18] G. Lipworth, A. Mrozack, J. Hunt, D. L. Marks, T. Driscoll, D. Brady, and D. R. Smith, "Metamaterial Apertures for Coherent Computational Imaging on the Physical Layer," *J. Opt. Soc. Am. A*, vol. 30, no. 8, pp. 1603–1612, 2013.

[19] J. Hunt, J. Gollub, T. Driscoll, G. Lipworth, A. Mrozack, M. S. Reynolds, D. J. Brady, and D. R. Smith, "Metamaterial Microwave Holographic Imaging System," *J. Opt. Soc. Am. A*, vol. 31, no. 10, pp. 2109–2119, 2014.

[20] L. Pulido-Mancera, T. Fromenteze, T. Sleasman, M. Boyarsky, M. F. Imani, M. Reynolds, and D. Smith, "Application of Range Migration Algorithms to Imaging with A Dynamic Metasurface Antenna," *J. Opt. Soc. Am. B*, vol. 33, no. 10, pp. 2082–2092, 2016.

[21] T. Sleasman, "Dynamic Metasurface Apertures for Computational Imaging," Ph.D. dissertation, Duke University, 2018.

[22] O. Yurduseven, M. F. Imani, H. Odabasi, J. N. Gollub, G. S. Lipworth, A. Rose, and D. R. Smith, "Resolution of the Frequency Diverse Metamaterial Aperture Imager," *Prog. Electromagn. Res.*, vol. 150, pp. 97–107, 2015.

[23] P. Isola, J.-Y. Zhu, T. Zhou, and A. A. Efros, "Image-to-Image Translation with Conditional Adversarial Networks," in *Proc. IEEE Conf. Comput. Vis. Pattern Recognit. (CVPR)*, 2017, pp. 5967–5976.

[24] A. Creswell, T. White, V. Dumoulin, K. Arulkumaran, B. Sengupta, and A. A. Bharath, "Generative Adversarial Networks: An Overview," *IEEE Signal Process. Mag.*, vol. 35, no. 1, pp. 53–65, 2018.

[25] I. Goodfellow *et al.*, "Generative adversarial nets," in *Proc. Adv. Neural Inf. Process. Syst.*, 2014, p. 2672–2680.

[26] Y. Bengio, P. Simard, and P. Frasconi, "Learning long-term dependencies with gradient descent is difficult," *IEEE Trans. Neural Netw.*, vol. 5, no. 2, pp. 157–166, 1994.

[27] X. Glorot and Y. Bengio, "Understanding the difficulty of training deep feedforward neural networks," in *Proc. Int. Conf. Artif. Intell. Statist.*, 2010.

[28] R. Parhi and R. D. Nowak, "The Role of Neural Network Activation Functions," *IEEE Signal Process. Lett.*, vol. 27, pp. 1779–1783, 2020.

[29] J. Ni, K. Shen, Y. Chen, W. Cao, and S. X. Yang, "An Improved Deep Network-Based Scene Classification Method for Self-Driving Cars," *IEEE Trans. Instrum. Meas.*, vol. 71, pp. 1–14, 2022.

[30] T. D. Nguyen, D. H. Kim, J. S. Yang, and S. Y. Park, "High-Speed ASIC Implementation of Tanh Activation Function Based on the CORDIC Algorithm," in *Proc. Int. Tech. Conf. Circuits/Syst. Comput. Commun. (ITC-CSCC)*, 2021, pp. 1–3.

[31] M. Kaloev and G. Krastev, "Comparative Analysis of Activation Functions Used in the Hidden Layers of Deep Neural Networks," in *Proc. Int. Congr. Human-Comput. Interact. Opt. Robot. Appl. (HORA)*, 2021, pp. 1–5.

[32] X. Wang, H. Ren, and A. Wang, "Smish: A Novel Activation Function for Deep Learning Methods," *Electronics*, vol. 11, no. 4, 2022.

[33] J. Laviada, G. Álvarez Narciandi, and F. Las-Heras, "Artifact Mitigation for High-Resolution Near-Field SAR Images by Means of Conditional Generative Adversarial Networks," *IEEE Trans. Instrum. Meas.*, vol. 71, pp. 1–11, 2022.

[34] C. Donciu and M. Temneanu, "An Alternative Method To Zero-padded DFT," *Measurement*, vol. 70, pp. 14–20, 2015.

[35] D. P. Kingma and J. Ba, "Adam: A Method for Stochastic Optimization," *CoRR*, vol. abs/1412.6980, 2014.

[36] W. Boulila, M. Driss, E. Alshanqiti, M. Al-Sarem, F. Saeed, and M. Krichen, *Weight Initialization Techniques for Deep Learning Algorithms in Remote Sensing: Recent Trends and Future Perspectives*, 2022, pp. 477–484.

[37] A. M. Molaei, S. Hu, V. Skouroliakou, V. Fusco, X. Chen, and O. Yurduseven, "Fast Processing Approach for Near-Field Terahertz Imaging With Linear Sparse Periodic Array," *IEEE Sens. J.*, vol. 22, no. 5, pp. 4410–4424, 2022.

[38] T. V. Hoang, V. Fusco, T. Fromenteze, and O. Yurduseven, "Dynamic Metasurface Antenna for Computational Polarimetric Imaging," in *Proc. Eur. Conf. Antennas Propag. (EuCAP)*, 2022, pp. 1–5.

[39] A. V. Balakrishnan and R. R. Mazumdar, "On Powers of Gaussian White Noise," *IEEE Trans. Inf. Theory*, vol. 57, no. 11, pp. 7629–7634, 2011.

[40] T. Sleasman, M. F. Imani, J. N. Gollub, and D. R. Smith, "Dynamic Metamaterial Aperture for Microwave Imaging," *Appl. Phys. Lett.*, vol. 107, no. 20, p. 204104, 2015.

[41] H. Zhao, S. Hu, H. Zhang, Z. Wang, H. Dong, P. del Hougne, T. J. Cui, and L. Li, "Intelligent Indoor Metasurface Robotics," *Natl. Sci. Rev.*, vol. 10, no. 8, 2022.